

## Article

# Unusual Water Flow in Ultra-Tight Porous Media: Integration of Profession and Innovation

Yanglu Wan <sup>1</sup>, Na Niu <sup>2,\*</sup>, Wei Lu <sup>1</sup>, Yushuang Zhou <sup>3</sup>, Bin Wang <sup>3</sup> and Shan Lu <sup>1</sup><sup>1</sup> School of Innovation and Entrepreneurship, Wuchang University of Technology, Wuhan 430200, China<sup>2</sup> Southwest Oil and Gas Company, SINOPEC, Chengdu 610041, China<sup>3</sup> Wuxi Research Institute of Petroleum Geology, SINOPEC, Wuxi 214126, China

\* Correspondence: wutxcxy@163.com

**Abstract:** Hydraulic fracturing is an effective method for stimulating reservoirs, making the economic development of ultra-tight shale gas and coalbed methane reservoirs possible. These formations are rich in nanopores, in which the fracturing fluid, such as fresh water, the flow, and the behavior of this flow differ significantly from those described in the classic Navier-Stokes formula. In bulk space, the interaction force exerted by the solid phase can be ignored, but the solid–fluid interaction plays a dominant role in nanoconfinement spaces in which the pore size is comparable to the molecular diameter. Nanoconfined water molecules tend to approach the water-wet pore surface, enhancing the water viscosity, which is a key parameter affecting the water flow capacity. Conversely, water molecules tend to stay in the middle of nanopores when subjected to a hydrophobic surface, leading to a decrease in viscosity. Thus, nanoconfined water viscosity is a function of the strength of the surface–fluid interaction, rather than a constant parameter, in classic theory. However, the influence of varying the viscosity on the nanoscale water flow behavior is still not fully understood. In this research, we incorporate wettability-dependent viscosity into a pore network modeling framework for stable flow for the first time. Our results show that: (a) the increase in viscosity under hydrophilic nanoconfinement could reduce the water flow capacity by as much as 11.3%; (b) the boundary slip is the primary mechanism for boosting the water flow in hydrophobic nanopores, as opposed to the slight enhancement contributed by a viscosity decline; and (c) water flow characterization in nanoscale porous media must consider both the pore size and surface wettability. Revealing the varying viscosity of water flow confined in nanopores can advance our microscopic understanding of water behavior and lay a solid theoretical foundation for fracturing-water invasion or flowback simulation.

**Keywords:** viscosity; nanoconfinement; wettability; pore network; simulation

**Citation:** Wan, Y.; Niu, N.; Lu, W.; Zhou, Y.; Wang, B.; Lu, S. Unusual Water Flow in Ultra-Tight Porous Media: Integration of Profession and Innovation. *Processes* **2023**, *11*, 1245. <https://doi.org/10.3390/pr11041245>

Academic Editors: Tao Zhang, Zheng Sun, Dong Feng, Hung Vo Thanh and Wen Zhao

Received: 28 March 2023

Revised: 13 April 2023

Accepted: 14 April 2023

Published: 18 April 2023



**Copyright:** © 2023 by the authors. Licensee MDPI, Basel, Switzerland. This article is an open access article distributed under the terms and conditions of the Creative Commons Attribution (CC BY) license (<https://creativecommons.org/licenses/by/4.0/>).

## 1. Introduction

In recent decades, advances in hydraulic fracturing technology have enabled the economic development of oil and gas resources from ultra-tight shale and coal [1–3]. The pores in shale can be broadly classified as organic and inorganic types, with pore sizes ranging between two and several hundred nanometers. Coal can be considered a composite medium consisting of a coal matrix and cleats [4,5], with cleat widths in the range of several microns and the pores in the matrix in the nanoscale range. During hydraulic fracturing, a large amount of fracturing fluid is injected into the shale or coal at high pressure, which can reach up to 50 MPa or more. As a result, water invasion unavoidably encounters the nanopores, and the water flow in the nanopores affects the overall invasion efficiency [6,7]. Nanoconfined fluids behave differently from conventional fluids in terms of their physical properties, such as the decline of the bubble point for hydrocarbon phase behavior in pores smaller than 20 nm [8–10]. The gas flow capacity through nanopores is also surprisingly higher than that evaluated by the classic Navier-Stokes (N-S) formula [11,12], with the magnitude exceeding several orders. Consequently,

conventional methods for describing water flow in nanopores can lead to inaccurate characterization, which requires further research.

The physical properties of nanoconfined water, including the viscosity and no-slip boundary conditions, are mainly governed by solid–fluid interactions, rather than intermolecular interactions in the bulk state. When water molecules are confined to a nanopore with a size comparable to their molecular diameter, the attraction or repulsive force induced by the surrounding pore wall cannot be ignored, which is fundamentally different from the precondition of the classic theoretical framework that is purely based on molecule–molecule interactions [13–15]. Therefore, focusing on the physical properties under solid–fluid interactions is crucial for understanding nanoconfined water flow behavior. Advanced experimental techniques have been used to directly examine water flow conductivity in nanotubes [16,17], indicating the inapplicability of the classic Navier-Stokes formula for describing nanoconfined water flow. Feibelman (2013) investigated the viscosity of water film on a kaolinite surface, a weak hydrophilic solid phase [18], using molecular simulation, and found that the water film viscosity was several times that of bulk water. Secchi (2016) experimentally examined the water flow capacity through a single nanotube [19] and found a significant enhancement in the flow efficiency compared to the conventional knowledge, which was attributed to a radius-dependent boundary slip as well as the viscosity variation. Using molecular dynamics, Thomas and McGaughey (2008) [20] simulated pressure-driven nanoconfined water flow and found that both the water viscosity in a nanopore and the slip length can be described as a function of the pore size. To understand the microscopic water molecular structure confined between two kaolinite surfaces, molecular dynamics simulations were performed, suggesting that the nanoconfined water viscosity could be one order larger than that of bulk water [21–23]. While the unusual alteration in the water viscosity confined inside nanopores has been recognized by both advanced experiments and molecular simulations, its impact on pressure-driven flow is still unclear. In addition to water viscosity variation, the boundary slip phenomenon, in which water molecules near the surface have some mobility, instead of always being stationary, in bulk water flow, must be incorporated to achieve a relatively accurate characterization of water flow at the nanoscale.

A great deal of effort has been devoted to investigating the behavior of water at the nanoscale [24–26]. However, little attention has been given to the water flow dynamics in porous media consisting of nanopores, which is crucial for understanding fracturing-water invasions inside a shale or coal matrix. A theoretical model for water flow in a nanopore was proposed, taking into account the surface wettability on the water viscosity variation and slip length. It suggests that the water flow capacity with a super-hydrophobic surface could be up to seven orders of magnitude stronger than that evaluated by the Hagen-Poiseuille equation [27]. Sun (2019) presented that the viscosity of the water close to the pore wall is extremely sensitive to surface–molecule interaction, while the water viscosity in the middle of the nanopore space is the same as bulk water [28]. In line with the continuum flow assumption, the water velocity profile at the nanoscale was analyzed, demonstrating the considerable effect of viscosity variation on the water flow capacity [29–31]. Molecular dynamics (MD) and the Lattice Boltzmann method (LBM) are widely utilized to explore nanoconfined water behavior [32–34]. However, the current fatal deficiency in MD research is the use of specific solid phase molecules to simulate the shale or coal nanopore surface [35–37], which fails to capture the surface–molecule interaction on the flow behavior of water confined in nanopores. Similarly, it is challenging to mimic the nanopore surface over a wide range of wettability using the LBM. Moreover, its time-consuming calculation and complex iteration hinder its applicability [38–40]. In regard to a shale or coal matrix, where the spatial pore structure is multi-factor-dependent and challenging to characterize, there is still no finite solution for pore network construction, although advanced approaches [41–43], including SEM image technology, CT scanning, as well as X-ray diffraction, are applied. Furthermore, the majority of pore network modeling (PNM) studies have focused on gas flow, while few studies on water flow have considered

the viscosity variation and boundary slip induced by the surface–molecule interaction. Therefore, a PNM investigation on water flow at the nanoscale is urgently needed, aiming to reveal the fracturing water invasion or flow-back behavior in a shale or coal matrix.

To clarify the research, the content is arranged as follows: First, a physical model illustrating the difference between nanoconfined water viscosity and bulk water is presented. Then, a theoretical model is developed based on the physical model to describe the water flow in a nanopore, taking into account the water viscosity variation and water slip at the boundary. Subsequently, a pore network model (PNM) is established to couple the spatial pore structure and the proposed pore-scale water flow model. The PNM is applied to identify the influence of the water viscosity, slip mechanism, and pore–structure evolution on the water flow capacity. Finally, several conclusions are drawn.

## 2. Model Description

The focus of this research is to investigate the effect of water viscosity variation on the water flow behavior in nanopores and nanoscale porous media. As shown in Figure 1, water viscosity is affected by surface wettability when water molecules are confined in a nano-space. In the bulk region, where the interaction force exerted by the pore surface can be neglected, the water viscosity is a function of the surrounding pressure and temperature [44,45]. However, for nanoconfined molecules, the surface–water interaction forces intensify, and water molecules tend to gather close to a hydrophilic surface, resulting in an increase in the water viscosity. Conversely, the repulsive force induced by a hydrophobic surface prevents water molecules from moving towards the surface, leading to a decrease in the water viscosity [46–48]. From a theoretical perspective, the interaction force by a mid-wet surface on water molecules is zero; therefore, the water viscosity remains the same as bulk water. Experimental findings in recent decades have shown that nanoconfined water flows surprisingly faster than bulk water, and this is attributed to the boundary slip phenomenon. This suggests that nanoconfined water molecules near the solid surface have fairly strong mobility, in contrast to the predictions made by the traditional N-S equation. Thus, the difference between nanoconfined water behavior and bulk water is evident [49,50]. Both the slip phenomenon and viscosity variation play prominent roles in affecting the water flow in nanopores, yet they have received little research attention. Additionally, an upscaling investigation on water flow in nanoscale porous media is rare, which solidifies the fundamental basis for revealing the fracturing fluid loss mechanisms and water production performance from shale reservoirs.

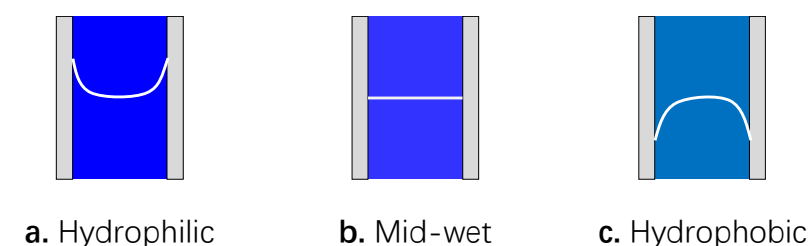


**Figure 1.** Water viscosity behavior inside nanopores with different wettability: (a) Hydrophilic surface; (b) Mid-wet surface; (c) Hydrophobic surface.

## 3. Model Establishment

To accurately simulate water flow behavior in porous media containing numerous nanopores, it is imperative to have a clear understanding of the water flow in a single nanopore. At the nanoscale, the slip phenomenon and viscosity variation are two prominent factors that affect water behavior and must be taken into account. The slip phenomenon describes the movement of water molecules close to the pore surface, while a viscosity change in nanoconfined water alters the flow resistance. Both the slip phenomenon and viscosity are known to be sensitive to temperature variation, but in order to focus on the

impact of unusual viscosity in this research, a constant temperature of 20 °C is used in this paper.

### 3.1. Nanoconfined Water Flow

In this section, the water flow capacity in a single nanopore is investigated, taking into account the effects of water viscosity variation and the boundary slip. The apparent permeability, which represents the water flow flux per displacement pressure difference, is derived, providing a basis for subsequent pore network modeling.

In regard to nanoconfined water viscosity, due to the limited distance where the fluid–surface interaction takes place, the viscosity of the water molecules close to the surface is drastically different compared to bulk water. In contrast, the water molecules away from the surface behave the same as bulk water. Therefore, the concept of the interfacial region, where unusual water viscosity occurs under nanoconfinement impact, is introduced in this work. The thickness of the interfacial region remains in debate, ranging between 0.5~1.5 nm, which is mainly related to the surface attributes and fluid type. In terms of the water molecules, the thickness is assigned as 0.7 nm, indicating that water molecules 0.7 nm away from the surface are beyond the control of the surface-induced force. Additionally, Wu et al. (2017) proposed a fancy correlation linking the surface contact angle to the water viscosity inside the interfacial region [27], and its reliability was verified by experimental data and molecular simulation results. It should be highlighted that the water viscosity in the whole interfacial region is regarded as a single value, instead of a varying parameter, in Wu et al. (2017). Actually, due to the close relationship between the fluid–surface interaction and water viscosity and the rapid rise in the interaction strength while water molecules approach the surface, the water viscosity will vary over the decreasing distance towards the surface. Utmost caution should be paid when using the correlation [27].

$$\mu_i = \mu_b(-0.018\theta + 3.25) \quad (1)$$

where  $\mu_i$  denotes the water viscosity in the interfacial region, cp;  $\mu_b$  denotes the bulk water viscosity, cp;  $\theta$  denotes the surface contact angle.

The geometry of nanopores has been found to affect the behavior of confined water, but for simplicity, this study focuses on cylindrical nanopores and does not consider the effects of geometry changes. Using Equation (1), the viscosity of the water molecules near the surface can be calculated, while the viscosity of the rest of the water molecules is assumed to be the same as that of bulk water. To determine the overall water viscosity within the entire nanopore, a volume-average method is proposed, which sums up the viscosity contributions from both the interfacial region and the rest of the nanopore based on their respective volumes.

$$\mu = \mu_i \frac{A_i(d)}{A_t(d)} + \mu_b \left[ 1 - \frac{A_i(d)}{A_t(d)} \right] \quad (2)$$

where  $\mu$  denotes the nanoconfined water viscosity, cp;  $d$  denotes the nanopore diameter, nm;  $A_i$  denotes the volume of the interfacial region, m<sup>3</sup>;  $A_t$  denotes the entire volume of the nanopore, m<sup>3</sup>.

The behavior of water in nanopores is affected by both the pore size and surface wettability, as demonstrated by the combination of Equations (1) and (2). In particular, the water viscosity in the interfacial region is highly sensitive to surface wettability, especially for nanopores with a size smaller than 10 nm, where the effect of wettability on the viscosity dominates. For larger nanopores, the impact of wettability on the nanoconfined water viscosity decreases significantly due to the smaller volume proportion of the interfacial region.

To quantify the slip phenomenon, the slip length is introduced, which represents the ratio of water molecular velocity to the shear rate at the boundary position. The strength of the slip phenomenon is determined by the slip length, with a longer slip length indicating a

stronger boundary slip. Molecular simulations and microscopic displacement experiments have confirmed the correlation between the slip length and nanopore size. In this work, the correlation describing the water slip length inside carbon nanotubes [20] is used, as the shale or coal matrix contains organic matter that can transform into graphene, a form of carbon nanotubes, under high geological thermal maturity.

$$L_s = L_\infty + \frac{C}{d^3} \quad (3)$$

where  $L_s$  denotes the slip length, nm;  $L_\infty$  denotes the water slip length on a perfect flat carbon sheet, nm;  $C$  is a fitted parameter, related to the surface properties and pore size. In this work, for the physical model of water flowing through carbon nanopores,  $L_\infty$  is 30 nm and  $C$  is equal to 352 nm<sup>4</sup>.

It has been reported that the continuum hydrodynamics theory remains valid for water flow in nanopores with a pore size of less than 2 nm [51,52]. Based on this, and taking into account the characterization of the nanoconfined water viscosity and slip length, the water flow equation at the nanoscale can be derived. The conventional water flow flux per pressure gradient in a pore with a pore diameter of  $d$  is provided first.

$$Q_c = \frac{\pi}{8\mu_b} (d/2)^4 \frac{dp}{dz} \quad (4)$$

where  $Q_c$  denotes the water flow flux using the conventional N-S equation, m<sup>3</sup>/s.

Considering the viscosity variation and boundary slip length, Equation (4) becomes the following equation.

$$Q_n = \frac{\pi}{8\mu} \left[ (d/2)^4 + 4(d/2)^3 L_s \right] \frac{dp}{dz} \quad (5)$$

where  $Q_n$  denotes the nanoconfined water flow flux, m<sup>3</sup>. In terms of a large pore size, the second term in the bracket of Equation (5) becomes negligible compared to the first term, and the nanoconfined water viscosity approaches bulk water viscosity; thus, Equation (5) can degenerate to Equation (4) successfully. In terms of nanopores, both the water viscosity and slip length affected by nanoconfinement are coupled in Equation (5), which could shed light on its discrepancy compared to the bulk water flow.

### 3.2. Pore Network Modeling

Water flow at the nanoscale can have important practical applications in various industries, such as the characterization of fracturing fluid loss or multiphase flow in the shale/coal matrix. However, upscaling the behavior of water flow from the nanoscale to the core scale is necessary to make it relevant to industry applications. Pore network modeling is a commonly used upscaling tool, where the core sample is considered to be a large number of nodes interconnected to each other, and the connections between any two nodes represent the nanopores. In this work, the nanopores were assigned specific pore sizes and surface contact angles. To establish the spatial pore network, the pore size distribution, which denotes the range of nanopore sizes, as well as the proportion of nanopores at each pore size, was provided. Furthermore, the co-ordination number, which denotes the number of nanopores that a single nanopore could connect to at the core scale, was also given. A higher co-ordination number implies a stronger connectivity of the constructed pore network. The spatial pore network was established using a self-coded program, based on the provided pore size distribution and co-ordination number.

This work focused on investigating stable water flow, rather than time-dependent flow issues. For a stable flow, the fluid pressure at each node in the developed pore network remains unchanged, as does the water flow flux in the nanopores. According to the mass conservation principle, the total water inflow flux towards a specified node should be equal to the water mass variation in the node. However, considering the stable

flow characteristics, there is no water mass variation in each node. Therefore, the control equation for the mass conservation of a node connecting  $n$  surrounding nodes is as follows:

$$\sum_{i=1}^{i=n} q_i = 0 \quad (6)$$

where  $q_i$  denotes the water mass flow flux from the  $i$  node to the calculation node, kg/s.

In Section 3.1, we investigated the capacity of nanoconfined water flow by considering the effects of the viscosity and slip length. By coupling the pressure difference between two connected nodes in the pore network, the mass flow flux can be calculated using the following expression.

$$q_i = \frac{\pi}{8\mu} \left[ (d/2)^4 + 4(d/2)^3 L_s \right] \frac{(P_i - P)}{L} \quad (7)$$

where  $P_i$  and  $P$  denote the node  $i$  pressure and calculation node pressure, respectively, MPa.

To obtain the water flow flux through the entire pore network, it is necessary to calculate the pressure of each node, which satisfies the correlation Equation (6). As the solutions for all nodes in the pore network are unique, the water flow flux can be obtained after solving all of the node pressures. The first step is to assign the inflow pressure and outflow pressure to the nodes located at the inlet and outlet of the pore network, respectively. Then, the pressure values ranging between the inlet pressure and outlet pressure are randomly generated, and the number of values is equal to the total number of nodes, excluding the inlet and outlet nodes. These generated pressure values are then assigned to the rest of the nodes, and each node has an initial pressure value. Next, the pressure of each node, except for the inlet and outlet nodes, is updated based on the mass conservation principle. During each iteration, the overall water flow flux is calculated after updating the pressure of all the nodes. The iteration continues until the difference in the water flow flux between successive pressure updates is within the desirable accuracy. The calculation procedures are illustrated in Figure 2. It should be noted that the calculation method is aimed at achieving a stable flow, and time-dependent flow issues are not considered in this work.

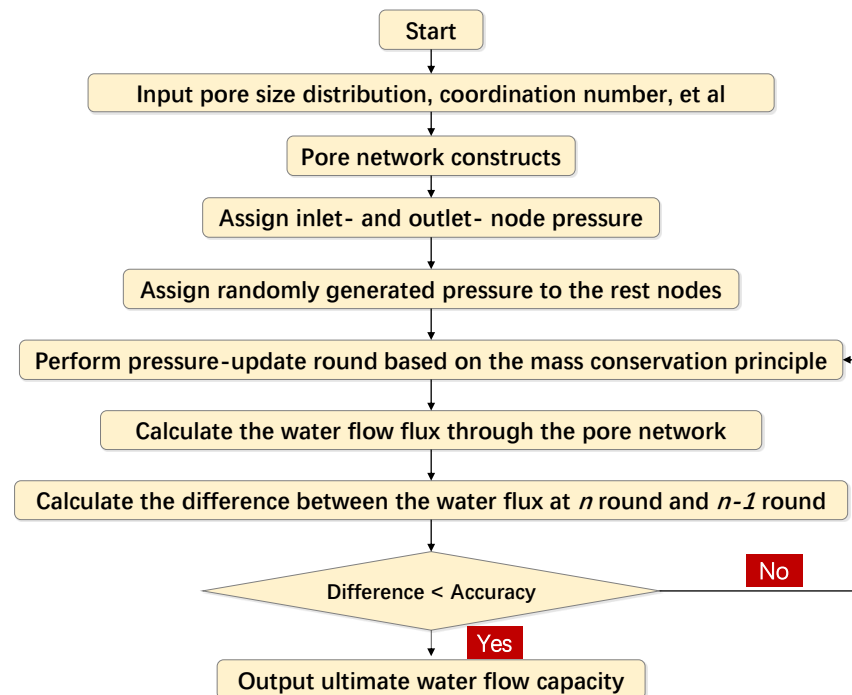


Figure 2. Calculation procedures for pore network modeling on stable water flow.

## 4. Results and Discussion

In this section, we aim to investigate the water flow behavior in nanoscale porous media while considering the effects of nanoconfinement, such as unusual water viscosity and the slip phenomenon. However, the spatial pore structure evolution characteristics in a shale or coal matrix add complexity to the accurate simulation of the water flow. To address this challenge, we use a pore network modeling approach that can reproduce the key parameters of porous media, such as the pore size distribution and co-ordination number. We also perform a sensitivity analysis to identify the influence of each influential factor on the water flow performance in the constructed pore network.

### 4.1. Nanoconfinement Effect

In this section, the focus is on quantifying the influential extent of the viscosity variation or boundary slip on the water flow capacity. Understanding this effect is essential to developing approaches that can enhance or contain water flow efficiency, depending on the dominant factor. For instance, if viscosity plays a prominent role in controlling the water flow under a specific condition, manipulating the water temperature to enhance or decline the water viscosity is a desirable method. On the other hand, surface modification becomes the effective approach when the boundary slip governs the water flow behavior. Thus, to gain insight into the nanoconfinement effect, the self-coded program developed for a stable water flow in the pore network in Section 3.2 is utilized.

The implemented pore network modeling couples the nanoscale water flow mechanisms discussed in Section 3.1, making it a unique approach. The pore size distribution is assigned to each nanopore in the constructed pore network, and the pore size ranges between 5~80 nm, which is a typical distribution for a shale or coal matrix. As depicted in Figure 3, the generated pore size distribution by the self-coded program has a favorable match with the assigned pore size distribution. This agreement verifies the reliability of the modeling results to some extent. The pore size distribution and co-ordination number remain unchanged to identify the impact of the water viscosity change subjected to the nanopores on the spatial pore characteristics. In this regard, the water flow performance is analyzed by varying the surface contact angle, which affects the boundary slip phenomenon. The quantification of the water flow capacity through porous media is conducted by utilizing the apparent permeability, which is the ratio of the cross-sectional water flow velocity to the pressure difference.

$$K = \frac{Q_{final} \mu_b L_t}{A(P_{inlet} - P_{outlet})} \quad (8)$$

where  $K$  denotes the apparent permeability, nD;  $Q_{final}$  denotes the final stable water flow flux, illustrated in Figure 2,  $m^3$ ;  $L_t$  denotes the total pore network length at the water flow direction, m;  $A$  denotes the flow cross-sectional area,  $m^2$ ;  $P_{inlet}$  and  $P_{outlet}$  denote the inlet pressure and outlet pressure, respectively.

The investigation in Figure 4 provides an insight into the impact of the surface contact angle on the water flow behavior. In this case, the surface contact angle of all the nanopores is the same, ranging between 0 and 180 degrees. The inherent permeability, as shown in Figure 4a, is constant at 5231 nD due to the assumption of the bulk water viscosity and no-slip hydrodynamic boundary condition, which overlooks the influence of the unusual water viscosity in the nanopores. However, the effect of the surface wettability on the apparent permeability is remarkable, particularly when the contact angle exceeds 100 degrees. The relationship between the apparent permeability and surface wettability can be divided into two parts based on the critical surface contact angle, which is 100 degrees.

When the contact angle is less than the critical value, indicating that the interaction force exerted by the surface on the water molecules is in attraction form, the apparent permeability gently enhances with the increasing contact angle. The apparent permeability may be less than the inherent permeability. On the other hand, the apparent permeability boosts when the contact angle exceeds the critical value, and the flow capacity could reach up to four orders of magnitude higher than the inherent permeability, indicating the super-

fast flow phenomenon as a result of the hydrophobic surface property. In this case, the surface imposes repulsive force on the water molecules to prevent their molecular approach to the surface, resulting in the decline of the whole water viscosity, and subsequently promoting water flow.

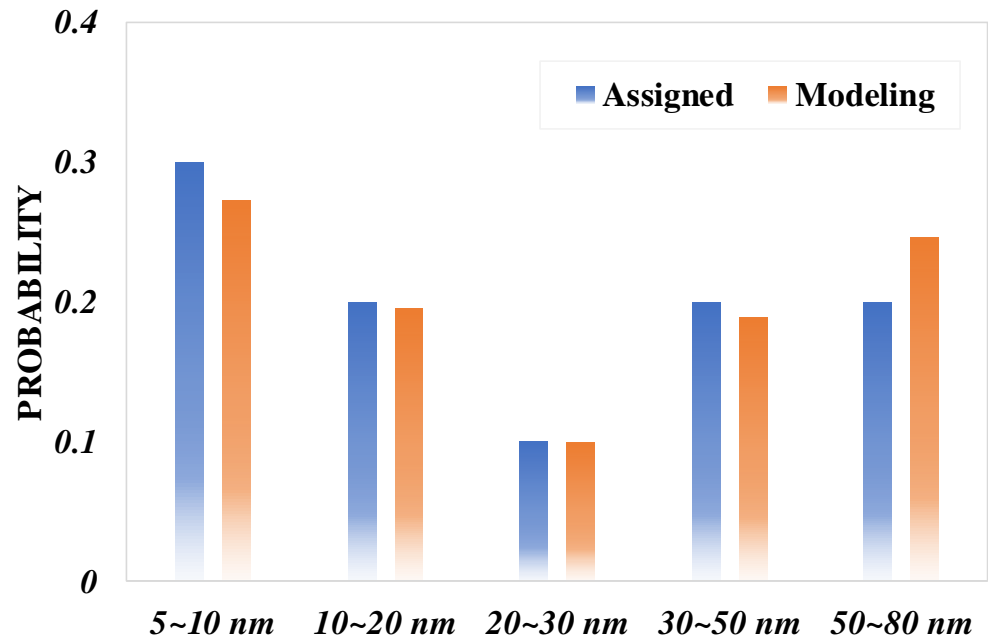


Figure 3. Comparison of the target pore size distribution and that generated by the program.

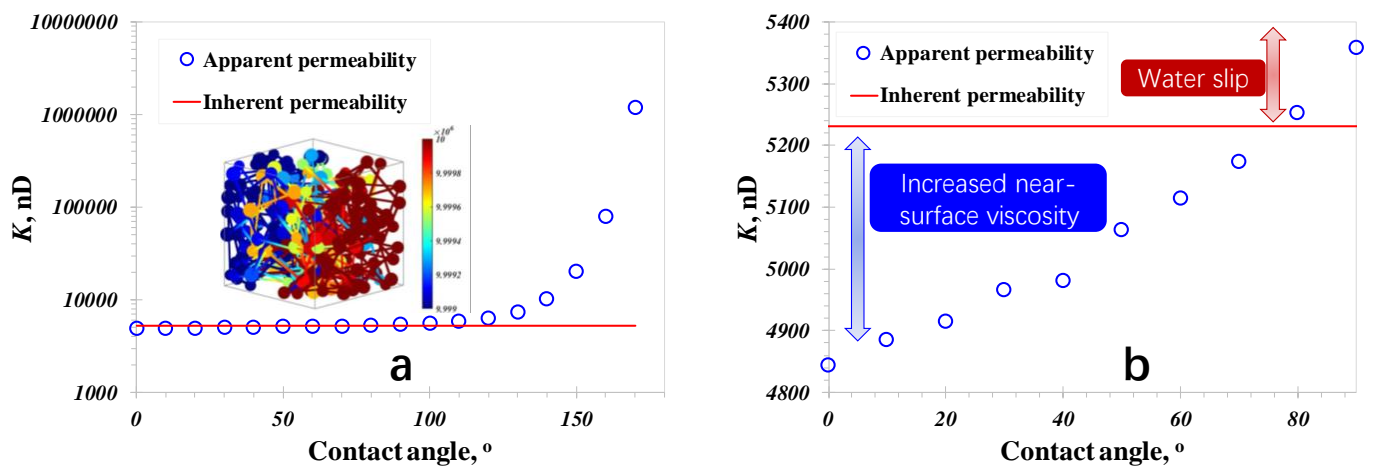
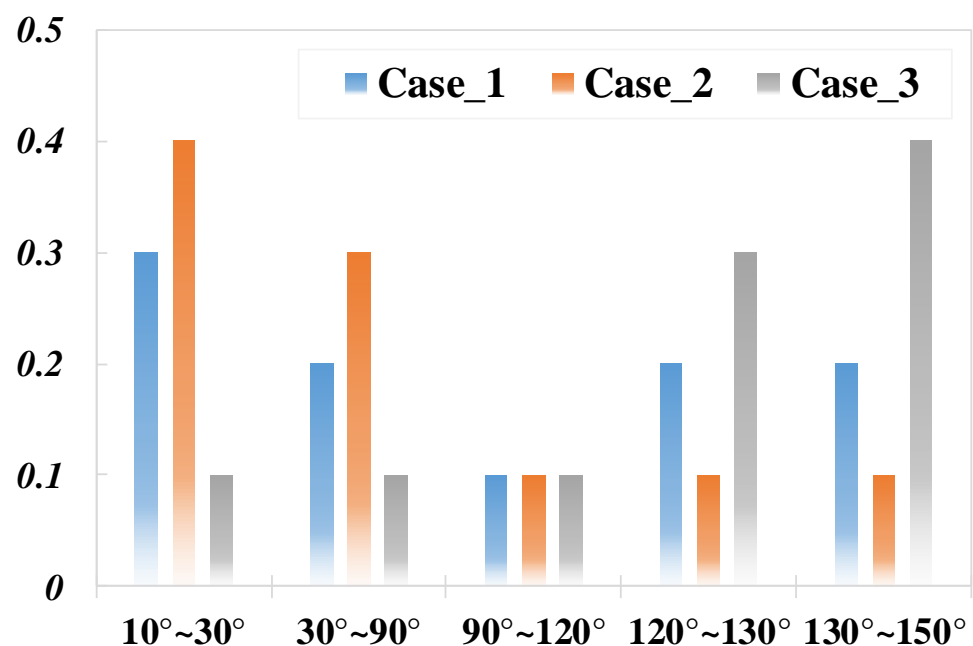


Figure 4. Water flow capacity in porous media consisting of nanopores: (a) Apparent permeability versus surface contact angle; (b) Underlying mechanism governing water flow capacity.

The permeability variation in the contact angle range, between 0 and 100 degrees, as presented in Figure 4b, shows that the apparent permeability is less than the inherent permeability when the contact angle is less than 80 degrees, which can be attributed to the increased viscosity in the hydrophilic nanopores. Moreover, the water slip contributes to the enhancement of the water flow capacity. The effect of the water slip length at the boundary is a function of the nanopore size, indicating that the slip length remains unchanged in this calculation case as the assigned pore size is unchanged. However, the idea that the impact of the boundary slip remains unchanged is misleading. According to the continuum flow theory, the viscosity variation affects the influence of the water slip. The constant slip length indicates the constant flow velocity of the water molecules at the boundary. The impact of the water slip enlarges with the decreasing water viscosity and declines with the

enhancing water viscosity on the water flow capacity. Therefore, the dramatic enhancement of the apparent permeability observed in Figure 4a is a result of both the water viscosity variation and water slip. It is insightful to recognize the changing role of the water slip with unusual water viscosity in nanopores.

To investigate the impact of the spatial porous characteristics on the water flow, a pore size of 20 nm was assigned to all nanopores in the constructed pore network. Three cases of surface wettability were then considered, as shown in Figure 5, and the associated apparent permeability for the water flow through the porous media was calculated. Case\_1 represented hydrophilic porous media, with 40% of the total nanopores having contact angles of less than 30 degrees. In contrast, Case\_3 represented hydrophobic porous media, where the water viscosity was significantly reduced. Case\_2 had the same surface wettability as the base case, which had a wide pore size distribution, shown in Figure 3, but with an unchanged pore size.



**Figure 5.** Surface contact angle variation range of nanopores in porous media.

As shown in Figure 6, the difference in the flow capacity between Case\_2 and the base case is relatively small, indicating that the pore size distribution has a limited effect on the flow capacity when the majority of the pore sizes are in the nanoscale range. The apparent permeability in Case\_2 is slightly stronger than the base case, which may be due to the fact that the average pore size in the base case is less than 20 nm. Additionally, larger pore sizes contribute to a stronger water flow capacity, assuming the same surface wettability feature. The apparent permeability for the water flow through the pore network increases in the order of Case\_2, Case\_1, and Case\_3. Similar to the water flow performance in nanopores, the water flow in nanopores with more hydrophobic surfaces can achieve a stronger flow efficiency. According to the surface contact angle distribution shown in Figure 5, 70% of the nanopores in Case\_3 have surface contact angles over 120°, which is much higher than in Case\_1 and Case\_2. As a result, the water flow resistance in the hydrophobic nanopores decreases dramatically, leading to the lowest overall resistance to water flow in Case\_3. Conversely, the porous media of Case\_2, consisting of many hydrophilic nanopores, imposes a lower water flow efficiency due to the higher water flow resistance.

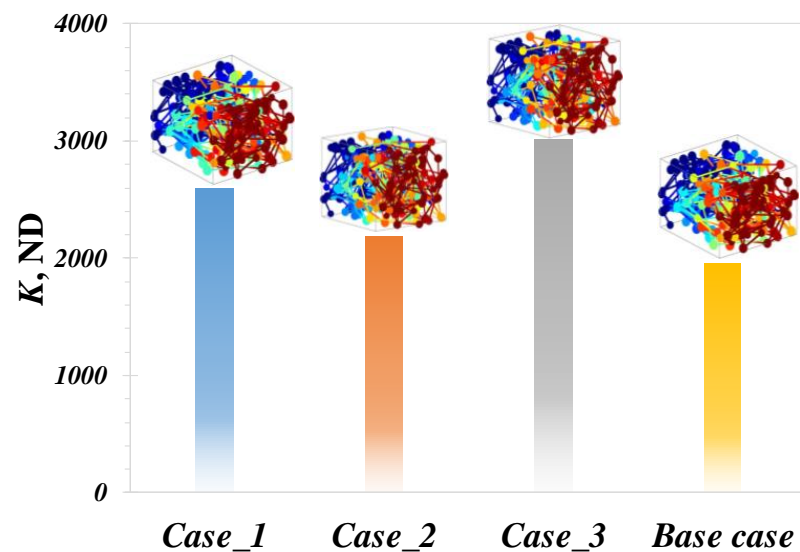


**Figure 6.** Wettability effect on apparent permeability for water flow at core scale.

#### 4.2. Pore Network Characteristics

Advanced experimental devices have made it possible to study the spatial evolution of pores in a coal or shale matrix as they vary with the geological depth and thermal maturity of the organic content. The ability to explore the complex spatial pore network characteristic and its related impact on fluid flow behavior is of utmost importance. To this end, numerous studies have been conducted to reproduce and present the spatial evolution characteristics of coal or shale matrix systems. In this article, we use an established pore network modeling tool coupled with nanoconfined water flow mechanisms to study the pore network characteristics, particularly the pore size distribution and co-ordination number, on water flow at the core scale. One of the primary objectives of this study is to understand the impact of the pore size distribution and co-ordination number on the fluid flow in coal or shale matrix systems. In this section, we focus on the impact of the surface contact angle of the nanopores in the pore network on the fluid flow. To exclude the effect of wettability, we set the surface contact angle of all the nanopores in the pore network to be  $80^\circ$ . This enabled us to study the effect of other pore network characteristics on the fluid flow without the confounding factor of varying wettability. The use of pore network modeling tools in conjunction with experimental techniques has enabled researchers to study the pore-scale mechanisms governing fluid flow in coal or shale matrix systems. The ability to control the wettability of the nanopores in the pore network provides a unique opportunity to study the impact of other pore network characteristics on the fluid flow, which can ultimately help to optimize the extraction of hydrocarbons from these systems.

In the exploration of the impact of pore size distribution on the fluid flow behavior, Figure 7 depicts three sets of pore size distributions. In these cases, other parameters describing the pore network, such as the positions of the nodes and the way the nodes connect to each other, remain unchanged. Specifically, Case\_1 presents a pore network where 70% of the nanopores have a pore size less than 20 nm, while 70% of the nanopores in the pore network of Case\_3 possess relatively large pore sizes, exceeding 30 nm. The simulation of water flow inside the pore network is then performed to identify the differences induced by varying the pore size distribution. As shown in Figure 8, it can be observed that the apparent permeability declines in the order of Case\_3, Case\_2, and Case\_1. In other words, the water flow capacity for Case\_3 is stronger than in Case\_2 and Case\_1 by as much as 18.3% and 51.7%, respectively, demonstrating the great positive effect of enlarging the pore size. Furthermore, the difference between Case\_2 and Case\_3 is far less than that between Case\_1 and Case\_2, indicating that enlarging the pore size could contribute more to the water flow efficiency when the average pore size is close to 10~20 nm than

when it approaches 50 nm. This finding suggests that a formation stimulation creating fractures or tremendously large pores could effectively advance the fluid flow capacity. The enhancement magnitude is more desirable for pore sizes less than 20 nm. The results of this study provide insights into the optimization of stimulation strategies for tight reservoirs. The formation of fractures or the creation of large pores can help to increase the average pore size and thus improve the water flow efficiency, particularly when the majority of the pore sizes are in the nanoscale range.

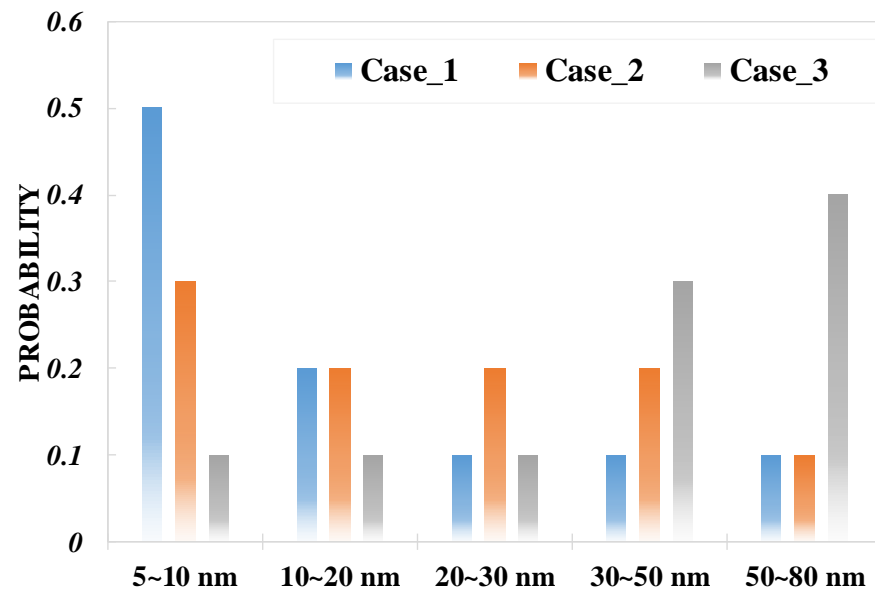


Figure 7. Different pore size distributions assigned to pore network.

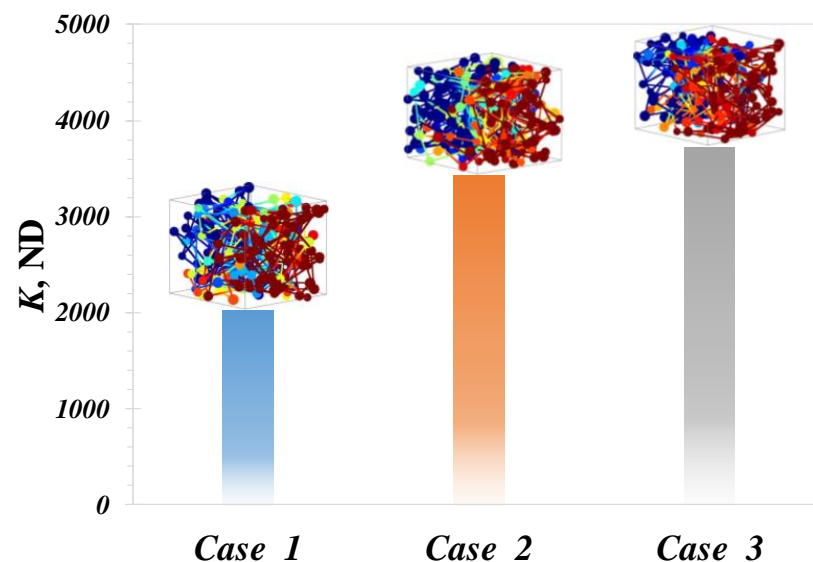
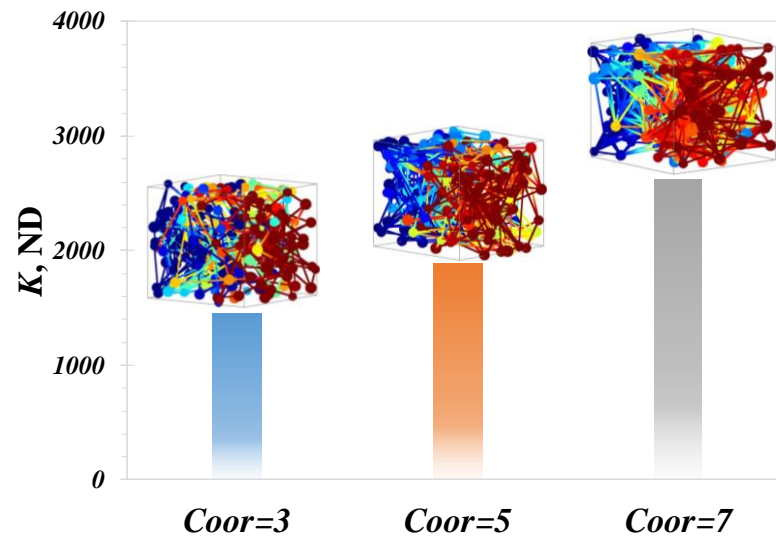


Figure 8. Impact of pore size distribution on apparent permeability.

In the construction process of the pore network, the co-ordination number plays a crucial role in determining the potential for water flow. The co-ordination number refers to the number of nodes that each node can connect to, and this parameter determines the availability of nanopores for water transport. The higher the co-ordination number, the more interconnected the pore network becomes, leading to enhanced water transport through the network. Therefore, increasing the co-ordination number can effectively improve the connectivity of the pore network, thereby promoting the water flow capacity in nanoscale porous media. In this study, the researchers kept all parameters of the

pore network constant, except for the co-ordination number. Figure 9 shows that the apparent permeability increases with an increase in the co-ordination number, confirming the importance of connectivity in promoting the water flow capacity. The findings of this study highlight the need to focus on improving the connectivity of nanoscale porous media to enhance their fluid flow behavior. By increasing the co-ordination number or finding other means to improve the connectivity, the potential for water transport through the pore network can be increased, leading to a more efficient and effective use of these porous media. Overall, these findings provide insights into the design and optimization of porous media for various applications, including energy and environmental engineering.



**Figure 9.** Impact of co-ordination number on apparent permeability.

## 5. Conclusions

- (1) We establish a model for the viscosity of water confined in nanoscale pores using the volume-average concept. This model considers variations in the viscosity occurring in the interfacial region and assumes bulk-like behavior in the rest of the region. Additionally, we develop a model for pore-scale water flow capacity and a pore network model that ensures a stable water flow. Both models are developed based on the continuum hydrodynamic principles.
- (2) The impact of hydrophilic and super-hydrophobic nanopore surfaces on water viscosity and permeability is significant. A hydrophilic surface leads to an increase in the viscosity and a decrease in the apparent permeability, while a super-hydrophobic surface results in a significant increase in the permeability due to a decline in the viscosity, coupled with the boundary slip phenomenon.
- (3) There are several methods for improving the water flow efficiency in nanoscale porous media, including enlarging the pore size, enhancing the co-ordination number, and modifying the surface properties to intensify the wettability. Enlarging the pore size contributes more significantly to the flow efficiency when the average pore size is close to 10–20 nm than when it approaches 50 nm.

**Author Contributions:** Investigation, Y.W.; supervision, N.N.; data curation, W.L.; draft preparation, Y.Z.; formal analysis, B.W.; validation, S.L. All authors have read and agreed to the published version of the manuscript.

**Funding:** This research was funded by National Natural Science Foundation of China grant number 52204031 and Natural Science Foundation of Sichuan Province grant number 23NSFSC4527. The APC was funded by 52204031.

**Institutional Review Board Statement:** Not applicable.

**Informed Consent Statement:** Not applicable.

**Data Availability Statement:** Data will be available on request.

**Acknowledgments:** This work was supported by the National Natural Science Foundation of China (Grant No. 52204031) and the Natural Science Foundation of Sichuan Province (Grant No. 23NS-FSC4527).

**Conflicts of Interest:** The authors declare no conflict of interest.

## References

1. Hou, B.; Chang, Z.; Fu, W.; Muhadasi, Y.; Chen, M. Fracture initiation and propagation in a deep shale gas reservoir subject to an alternating-fluid-injection hydraulic-fracturing treatment. *SPE J.* **2019**, *24*, 1839–1855. [[CrossRef](#)]
2. Huang, T.; Li, Z.; Mayer, B.; Nightingale, M.; Li, X.; Li, G.; Long, Y.; Pang, Z. Identification of geochemical processes during hydraulic fracturing of a shale gas reservoir: A controlled field and laboratory water-rock interaction experiment. *Geophys. Res. Lett.* **2020**, *47*, e2020GL090420. [[CrossRef](#)]
3. Sun, Z.; Huang, B.; Liu, Y.; Jiang, Y.; Zhang, Z.; Hou, M.; Li, Y. Gas-phase production equation for CBM reservoirs: Interaction between hydraulic fracturing and coal orthotropic feature. *J. Pet. Sci. Eng.* **2022**, *213*, 110428. [[CrossRef](#)]
4. Akhondzadeh, H.; Keshavarz, A.; Al-Yaseri, A.Z.; Ali, M.; Awan, F.U.; Wang, X.; Yang, Y.; Iglauer, S.; Lebedev, M. Pore-scale analysis of coal cleat network evolution through liquid nitrogen treatment: A Micro-Computed Tomography investigation. *Int. J. Coal Geol.* **2020**, *219*, 103370. [[CrossRef](#)]
5. Roslin, A.; Pokrajac, D.; Zhou, Y. Cleat structure analysis and permeability simulation of coal samples based on micro-computed tomography (micro-CT) and scan electron microscopy (SEM) technology. *Fuel* **2019**, *254*, 115579. [[CrossRef](#)]
6. Wijaya, N.; Sheng, J.J. Mitigating near-fracture blockage and enhancing oil recovery in tight reservoirs by adding surfactants in hydraulic fracturing fluid. *J. Pet. Sci. Eng.* **2020**, *185*, 106611. [[CrossRef](#)]
7. Fernandez, C.A.; Gupta, V.; Dai, G.L.; Kuprat, A.P.; Bonneville, A.; Appriou, D.; Horner, J.A.; Martin, P.F.; Burghardt, J.A. Insights into a greener stimuli-responsive fracturing fluid for geothermal energy recovery. *ACS Sustain. Chem. Eng.* **2019**, *7*, 19660–19668. [[CrossRef](#)]
8. Chen, S.; Jiang, J.; Guo, B. A pore-network-based upscaling framework for the nanoconfined phase behavior in shale rocks. *Chem. Eng. J.* **2021**, *417*, 129210. [[CrossRef](#)]
9. Sun, Z.; Wang, S.; Xiong, H.; Wu, K.; Shi, J. Optimal nanocone geometry for water flow. *AIChE J.* **2022**, *68*, e17543. [[CrossRef](#)]
10. Sun, Z.; Huang, B.; Yan, S.; Wang, S.; Wu, K.; Yu, W.; Li, Y.; Wang, S. Nanoconfined methane thermodynamic behavior below critical temperature: Liquid–vapor coexistence curve under wettability effect. *Ind. Eng. Chem. Res.* **2022**, *61*, 4971–4979. [[CrossRef](#)]
11. Yang, X. Numerical approximations of the Navier–Stokes equation coupled with volume-conserved multi-phase-field vesicles system: Fully-decoupled, linear, unconditionally energy stable and second-order time-accurate numerical scheme. *Comput. Methods Appl. Mech. Eng.* **2021**, *375*, 113600. [[CrossRef](#)]
12. Coron, J.M.; Marbach, F.; Sueur, F.; Zhang, P. Controllability of the Navier–Stokes equation in a rectangle with a little help of a distributed phantom force. *Ann. PDE* **2019**, *5*, 17. [[CrossRef](#)]
13. Gong, C.; Sun, S.; Zhang, Y.; Sun, L.; Su, Z.; Wu, A.; Wei, G. Hierarchical nanomaterials via biomolecular self-assembly and bioinspiration for energy and environmental applications. *Nanoscale* **2019**, *11*, 4147–4182. [[CrossRef](#)]
14. Geagea, E.; Jeannotot, J.; Morgenthaler, L.; Lamare, S.; Palmino, F.; Chérioux, F. On-Surface Synthesis of Ligands to Elaborate Coordination Polymers on an Au (111) Surface. *Nanomaterials* **2021**, *11*, 2102. [[CrossRef](#)]
15. Wang, L.; Gong, C.; Yuan, X.; Wei, G. Controlling the self-assembly of biomolecules into functional nanomaterials through internal interactions and external stimulations: A review. *Nanomaterials* **2019**, *9*, 285. [[CrossRef](#)]
16. Shrestha, R.G.; Kubota, Y.; Sakamoto, Y.; Kawakita, J. Quick and sensitive detection of water using galvanic-coupled arrays with a submicron gap for the advanced prediction of dew condensation. *Sensors* **2020**, *20*, 3314. [[CrossRef](#)]
17. Mekawy, M.; Noguchi, H.; Kawakita, J. Quantitative and qualitative studies for real monitoring of interfacial molecular water. *J. Colloid Interface Sci.* **2022**, *613*, 311–319. [[CrossRef](#)]
18. Feibelman, P.J. Viscosity of ultrathin water films confined between aluminol surfaces of kaolinite: Ab initio simulations. *J. Phys. Chem. C* **2013**, *117*, 6088–6095. [[CrossRef](#)]
19. Secchi, E.; Marbach, S.; Niguès, A.; Stein, D.; Siria, A.; Bocquet, L. Massive radius-dependent flow slippage in carbon nanotubes. *Nature* **2016**, *537*, 210–213. [[CrossRef](#)]
20. Thomas, J.A.; McGaughey, A.J. Reassessing fast water transport through carbon nanotubes. *Nano Lett.* **2008**, *8*, 2788–2793. [[CrossRef](#)]
21. Haria, N.R.; Grest, G.S.; Lorenz, C.D. Viscosity of nanoconfined water between hydroxyl basal surfaces of kaolinite: Classical simulation results. *J. Phys. Chem. C* **2013**, *117*, 6096–6104. [[CrossRef](#)]
22. Bakli, C.; Chakraborty, S. Anomalous interplay of slip, shear and wettability in nanoconfined water. *Nanoscale* **2019**, *11*, 11254–11261. [[CrossRef](#)] [[PubMed](#)]
23. Deisenbeck, F.; Freysoldt, C.; Todorova, M.; Neugebauer, J.; Wippermann, S. Dielectric properties of nanoconfined water: A canonical thermopotentiostat approach. *Phys. Rev. Lett.* **2021**, *126*, 136803. [[CrossRef](#)] [[PubMed](#)]

24. Pan, J.; Xiao, S.; Zhang, Z.; Wei, N.; He, J.; Zhao, J. Nanoconfined water dynamics in multilayer graphene nanopores. *J. Phys. Chem. C* **2020**, *124*, 17819–17828. [[CrossRef](#)]
25. Zhao, Z.; Xue, M.; Qiu, H.; Guo, W.; Zhang, Z. Giant mechanocaloric effect of nanoconfined water near room temperature. *Cell Rep. Phys. Sci.* **2022**, *3*, 100822. [[CrossRef](#)]
26. Moid, M.; Finkelstein, Y.; Moreh, R.; Maiti, P.K. Microscopic study of proton kinetic energy anomaly for nanoconfined water. *J. Phys. Chem. B* **2019**, *124*, 190–198. [[CrossRef](#)]
27. Wu, K.; Chen, Z.; Li, J.; Li, X.; Xu, J.; Dong, X. Wettability effect on nanoconfined water flow. *Proc. Natl. Acad. Sci. USA* **2017**, *114*, 3358–3363. [[CrossRef](#)]
28. Sun, Z.; Wu, K.; Shi, J.; Zhang, T.; Feng, D.; Huang, L.; Li, X. An analytical model for transport capacity of water confined in nanopores. *Int. J. Heat Mass Transf.* **2019**, *138*, 620–630. [[CrossRef](#)]
29. Corti, H.R.; Appignanesi, G.A.; Barbosa, M.C.; Bordin, J.R.; Calero, C.; Camisasca, G.; Elola, M.D.; Franzese, G.; Gallo, P.; Hassanali, A.; et al. Structure and dynamics of nanoconfined water and aqueous solutions. *Eur. Phys. J. E* **2021**, *44*, 136. [[CrossRef](#)]
30. Kapil, V.; Schran, C.; Zen, A.; Chen, J.; Pickard, C.J.; Michaelides, A. The first-principles phase diagram of monolayer nanoconfined water. *Nature* **2022**, *609*, 512–516. [[CrossRef](#)]
31. Paniagua-Guerra, L.E.; Gonzalez-Valle, C.U.; Ramos-Alvarado, B. Effects of the interfacial modeling approach on equilibrium calculations of slip length for nanoconfined water in carbon slits. *Langmuir* **2020**, *36*, 14772–14781. [[CrossRef](#)]
32. Cheng, Z.; Ning, Z.; Kang, D.H. Lattice Boltzmann simulation of water flow through rough nanopores. *Chem. Eng. Sci.* **2021**, *236*, 116329. [[CrossRef](#)]
33. Rao, Q.; Xia, Y.; Li, J.; Deo, M.; Li, Z. Flow reduction of hydrocarbon liquid in silica nanochannel: Insight from many-body dissipative particle dynamics simulations. *J. Mol. Liq.* **2021**, *344*, 117673. [[CrossRef](#)]
34. Lubbers, N.; Agarwal, A.; Chen, Y.; Son, S.; Mehana, M.; Kang, Q.; Karra, S.; Junghans, C.; Germann, T.C.; Viswanathan, H.S. Modeling and scale-bridging using machine learning: Nanoconfinement effects in porous media. *Sci. Rep.* **2020**, *10*, 13312. [[CrossRef](#)]
35. Jin, L.; Zhou, L.; Du, X. A Molecular Analysis of Critical Factors for Interface and Size Effects on Heat Conduction in Nanoconfined Water Film. *J. Therm. Sci.* **2022**, *31*, 1155–1166. [[CrossRef](#)]
36. Lynch, C.I.; Klesse, G.; Rao, S.; Tucker, S.J.; Sansom, M.S. Water nanoconfined in a hydrophobic pore: Molecular dynamics simulations of transmembrane protein 175 and the influence of water models. *ACS Nano* **2021**, *15*, 19098–19108. [[CrossRef](#)]
37. Sun, Z.; Li, X.; Liu, W.; Zhang, T.; He, M.; Nasrabadi, H. Molecular dynamics of methane flow behavior through realistic organic nanopores under geologic shale condition: Pore size and kerogen types. *Chem. Eng. J.* **2020**, *398*, 124341. [[CrossRef](#)]
38. Santos, J.E.; Mehana, M.; Wu, H.; Prodanovic, M.; Kang, Q.; Lubbers, N.; Viswanathan, H.; Pyrcz, M.J. Modeling nanoconfinement effects using active learning. *J. Phys. Chem. C* **2020**, *124*, 22200–22211. [[CrossRef](#)]
39. Yi, J.; Liu, L.; Xia, Z.; Wang, J.; Jing, Y.; Duan, L. Effects of wettability on relative permeability of rough-walled fracture at pore-scale: A lattice Boltzmann analysis. *Appl. Therm. Eng.* **2021**, *194*, 117100. [[CrossRef](#)]
40. Sun, Z.; Li, X.; Shi, J.; Zhang, T.; Sun, F. Apparent permeability model for real gas transport through shale gas reservoirs considering water distribution characteristic. *Int. J. Heat Mass Transf.* **2017**, *115*, 1008–1019. [[CrossRef](#)]
41. Blunt, M.J.; Jackson, M.D.; Piri, M.; Valvatne, P.H. Detailed physics, predictive capabilities and macroscopic consequences for pore-network models of multiphase flow. *Adv. Water Resour.* **2002**, *25*, 1069–1089. [[CrossRef](#)]
42. Joekar-Niasar, V.; Hassanizadeh, S.M. Analysis of fundamentals of two-phase flow in porous media using dynamic pore-network models: A review. *Crit. Rev. Environ. Sci. Technol.* **2012**, *42*, 1895–1976. [[CrossRef](#)]
43. Medici, E.F.; Zenyuk, I.V.; Parkinson, D.Y.; Weber, A.Z.; Allen, J.S. Understanding Water Transport in Polymer Electrolyte Fuel Cells Using Coupled Continuum and Pore-Network Models. *Fuel Cells* **2016**, *16*, 725–733. [[CrossRef](#)]
44. Shaat, M. Viscosity of water interfaces with hydrophobic nanopores: Application to water flow in carbon nanotubes. *Langmuir* **2017**, *33*, 12814–12819. [[CrossRef](#)]
45. Nalaparaju, A.; Wang, J.; Jiang, J. Enhancing water permeation through alumina membranes by changing from cylindrical to conical nanopores. *Nanoscale* **2019**, *11*, 9869–9878. [[CrossRef](#)]
46. Martyushev, D.A.; Ponomareva, I.N.; Chukhlov, A.S.; Davoodi, S.; Osovetsky, B.M.; Kazymov, K.P.; Yang, Y. Study of void space structure and its influence on carbonate reservoir properties: X-ray microtomography, electron microscopy, and well testing. *Mar. Pet. Geol.* **2023**, *151*, 106192. [[CrossRef](#)]
47. Rashid, M.; Luo, M.; Ashraf, U.; Hussain, W.; Ali, N.; Rahman, N.; Hussain, S.; Martyushev, D.A.; Vo Thanh, H.; Anees, A. Reservoir Quality Prediction of Gas-Bearing Carbonate Sediments in the Qadirpur Field: Insights from Advanced Machine Learning Approaches of SOM and Cluster Analysis. *Minerals* **2023**, *13*, 29. [[CrossRef](#)]
48. Galkin, S.V.; Martyushev, D.A.; Osovetsky, B.M.; Kazymov, K.P. Huaisen Song Evaluation of void space of complicated potentially oil-bearing carbonate formation using X-ray tomography and electron microscopy methods. *Energy Rep.* **2022**, *8*, 6245–6257. [[CrossRef](#)]
49. Cong, Z.; Li, Y.; Tang, J.; Martyushev, D.A.; Yang, F. Numerical simulation of hydraulic fracture height layer-through propagation based on three-dimensional lattice method. *Eng. Fract. Mech.* **2022**, *264*, 108331. [[CrossRef](#)]
50. Makarian, E.; Abad, A.B.M.N.; Manaman, N.S.; Mansourian, D.; Elyasi, A.; Namazifard, P.; Martyushev, D. An efficient and comprehensive poroelastic analysis of hydrocarbon systems using multiple data sets through laboratory tests and geophysical logs: A case study in an Iranian hydrocarbon reservoir. *Carbonates Evaporites* **2023**, *38*, 37. [[CrossRef](#)]

51. Zhang, T.; Zhang, L.; Zhao, Y.; Zhang, R.; Zhang, D.; He, X.; Ge, F.; Wu, J.; Javadpour, F. Ganglia dynamics during imbibition and drainage processes in nanoporous systems. *Phys. Fluids* **2022**, *34*, 042016. [[CrossRef](#)]
52. Zhang, T.; Zhang, B.; Zhao, Y.; Javadpour, F.; He, X.; Ge, F.; Wu, J.; Zhang, D. Simulation of water flow in a nanochannel with a sudden contraction or expansion. *Langmuir* **2022**, *38*, 6720–6730. [[CrossRef](#)]

**Disclaimer/Publisher's Note:** The statements, opinions and data contained in all publications are solely those of the individual author(s) and contributor(s) and not of MDPI and/or the editor(s). MDPI and/or the editor(s) disclaim responsibility for any injury to people or property resulting from any ideas, methods, instructions or products referred to in the content.